International Journal of Adhesion and Adhesives
April 2016, Volume 66, Pages 147-159
http://dx.doi.org/10.1016/j.ijadhadh.2016.01.001
http://archimer.ifremer.fr/doc/00308/41956/

Investigating the fracture behavior of adhesively bonded metallic joints using the Arcan fixture

Stamoulis G. [1, *], Carrere N. [2], Cognard J.-Y. [2], Davies Peter [3], Badulescu C. [2]

[1] Laboratoire Brestois de Mécanique et des Systèmes (EA4325), ENSTA/UBO/ENIB, UBO, IUT de Brest – GMP, Rue de Kergoat - CS 93837, 29238 Brest Cedex 3, France
[2] Laboratoire Brestois de Mécanique et des Systèmes (EA4325), ENSTA/UBO/ENIB, ENSTA-Bretagne, 2 rue François Verny, 29806 Brest Cedex 9, France
[3] Marine Structures Laboratory, IFREMER, Centre de Bretagne, France B.P. 70, 29280 Plouzané Cedex, France

* Corresponding author : Georgios Stamoulis, email address : georgios.stamoulis@univ-brest.fr

Abstract :

In the present study, the fracture behavior of a crash optimized adhesive was examined by means of the Arcan fixture. The specimens were prepared using substrates of Aluminum 2017 A and two pre-cracks (one per each extremity of the joint) were created. The section of the substrates has been specially designed to stabilize crack propagation. The thickness of the adhesive layer was fixed at 0.5 mm. The tests were performed in the mixed mode I/II plane and under compression/shear load, at a speed of 0.5 mm/min. To avoid measuring the crack length during the experiments, an alternative methodology to calculate the fracture toughness is proposed. The results are in good accordance with previously published data on the same adhesive using “classical” TDCB (Tapered Double Cantilever Beam) and MMB (Mixed Mode Bending) tests. The influence of compression/shear loading on the fracture properties of the joint is also discussed.

Keywords : Arcan Fixture, Structural Adhesives, Linear Elastic Fracture Mechanics, Fracture Toughness, Finite Element Analysis

1. Introduction

In modern industry, the use of adhesives to bond dissimilar materials is very popular in various application fields like aeronautics, automobile or marine systems. The strength of the bonded structure can be predicted by means of the fracture mechanics based theory. In such case, it is needed to measure the critical strain energy release rate or fracture toughness (GC) of the adhesive, which denotes the potential energy dissipated to propagate a crack inside a solid medium over a unit area. If the GC of the adhesive is known, it can also be used in Cohesive Zone models to predict crack propagation in structures [1]. The value of GC strongly depends on three loading states at the end of the crack tip: mode I (the tensile opening mode), mode II (the in-plane shear mode) and mode III (the anti

plane shear mode).

The extensive work performed by many research teams to study the mode I fracture toughness (GIC) of structural adhesives has led to the establishment of standard types of tests for this failure mode [2-4]: the DCB (Double Cantilever Beam) and the TDCB (Tapered Double Cantilever Beam). Unlike mode I, no formal standardized tests exist to study mixed mode I/II and mode II fracture behaviors of structural adhesives. However, for these two cases, there exist standardized tests for composite materials: the MMB (Mixed Mode Bending) [5], the CELS (Calibrated End-Loaded Split) [6] and the ENF (End Notched Flexure) [7] tests. These tests can be implemented to study the fracture resistance of structural adhesives too. Examples

of use of the MMB test to study the mixed mode I/II fracture behavior of adhesives can be found in [8-9], and of other types of specimen geometries in [10]. Davies et al. [11] presented an international round robin to examine the mode II interlaminar fracture toughness of carbon fiber reinforced epoxy composites involving, apart from the ENF, the 4ENF (four point ENF), the SENF (Stabilized ENF) and the ELS (End-Loaded Split) tests. Some limitations of the methods are also reported in the same study. The study of the failure of structural adhesives under mode III is generally of less importance [12] and out of the scope of the present paper. An example of a testing procedure for this failure mode can be found in [13].

All the previous "classical" tests make use of the LEFM (Linear Elastic Fracture Mechanics) theory to calculate the fracture toughness G_C of structural adhesives. They necessitate a stable propagation of the crack. In most cases, substrates with a very high limit of elasticity are required, as any important non-linear behavior of the adherents can easily lead to erroneous results. Moreover, the value of G_C depends on the proper experimental measurement of the crack length value. This is very difficult to accomplish, particularly when shear is present, due to the nucleation of micro-cracks ahead of the crack tip. Although there exist some alternatives to overcome this last problem [14-15], improvement is still needed. Finally, it must also be noted that "classical" tests do not take into account all possible solicitation modes of adhesively bonded structures, as for example compression-shear loadings.

One of the alternatives to calculate the fracture toughness G_C of adhesive joints is to use the Arcan fixture [16]. A schematization of the principle of the Arcan method is shown in figure 1a. This method is particularly suitable to load a material or a bonded structure at different ratios in the mixed mode I/II plane, by simply varying the loading phase angle γ from 0^o (pure tensile load) to 90^o (pure shear load). There exist, however, some modified versions allowing

solicitations of the tested material until 135° [17] (compression-shear load, figure 1b) and until 180° [18] (pure compression load). Although the Arcan fixture has been used several times in the past to study crack growth in homogenous materials in order to define mixed mode I/II failure criterions, as for example by Sutton et al. [19-20], and also for composites [21], it has rarely been used by researchers to define full fracture envelopes of adhesive joints. In 1995, Pang [22] proposed the Compact Mixed Mode (CMM) specimen geometry together with the Arcan fixture to determine the fracture resistance of adhesive joints using metallic substrates. This methodology was used later on [23] to investigate also the effects of the layer thickness and the crack length ratio. By means of a similar to the CMM specimen geometry, Choupani studied the adhesive and cohesive fracture characteristics of adhesive joints [24-25], and also of laminated composite material [26]. An interface fracture specimen to use with the Arcan fixture in order to study the failure of adhesively bonded structures can be found in [27]. In all of these specimen geometries however, no stable crack propagation has been reported before total rupture. In addition, no comparisons with "classical" fracture mechanics tests have been attempted, and no investigations have been performed as far as the effect of compression/shear load on the values of the fracture toughness is concerned.

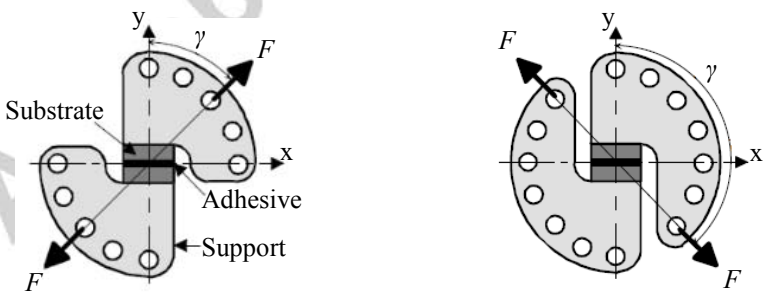

Figure 1: Schematization of the principles of the: a) Arcan fixture, b) modified Arcan fixture (γ : phase angle, F : load direction) [17].

In an attempt to provide answers to the previous issues, the modified Arcan fixture (figure 1b) was used to measure the fracture properties of a crash optimized single-compound epoxy adhesive SikaPower®-498. These properties for the same adhesive have been also examined in the past [28, 9] using "classical" TDCB, MMB and ENF tests. As it was shown in [9], the mixed mode I/II fracture characteristics of the adhesive under investigation can be adequately described by the Benzeggagh-Kenane [29] failure criterion. In the present manuscript, the results of [9] are compared with the corresponding ones from the Arcan fixture, and an alternative procedure to investigate the failure properties of adhesive joints is illustrated. This procedure consists of fabricating substrates with a special section to allow crack propagation, and of a methodology to calculate the fracture toughness combining digital image correlation measurements and finite element modelling of the tests. The latter can be used to bypass the need for experimental measurement of the value of the crack length, and also perform the necessary mode partitioning. In addition, the results for the fracture toughness of the adhesive under investigation when submitted to compression/shear load are also reported.

2. Preparation of the specimens

The material of the substrates and the parameters of the bonding procedure were chosen to be similar to [9], in order to allow for a coherent comparison between the results of the TDCB-MMB tests and those of the Arcan fixture. Thus, substrates of Aluminum 2017A were used to make the bonded assembly. The form and dimensions of these substrates are shown in figure 2a. Their sections were wider in the middle (20 mm) than at the two extremities (5 mm). They have been specially designed to stabilize, during the tests, the propagation of the pre-cracks located at the two extremities of the specimen (figure 2b).

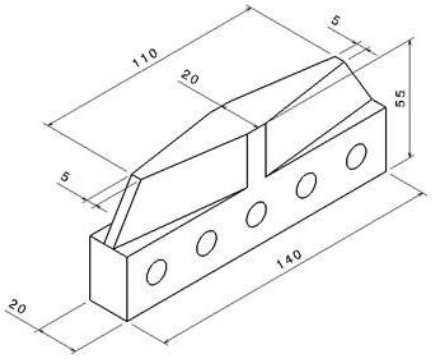

(a)

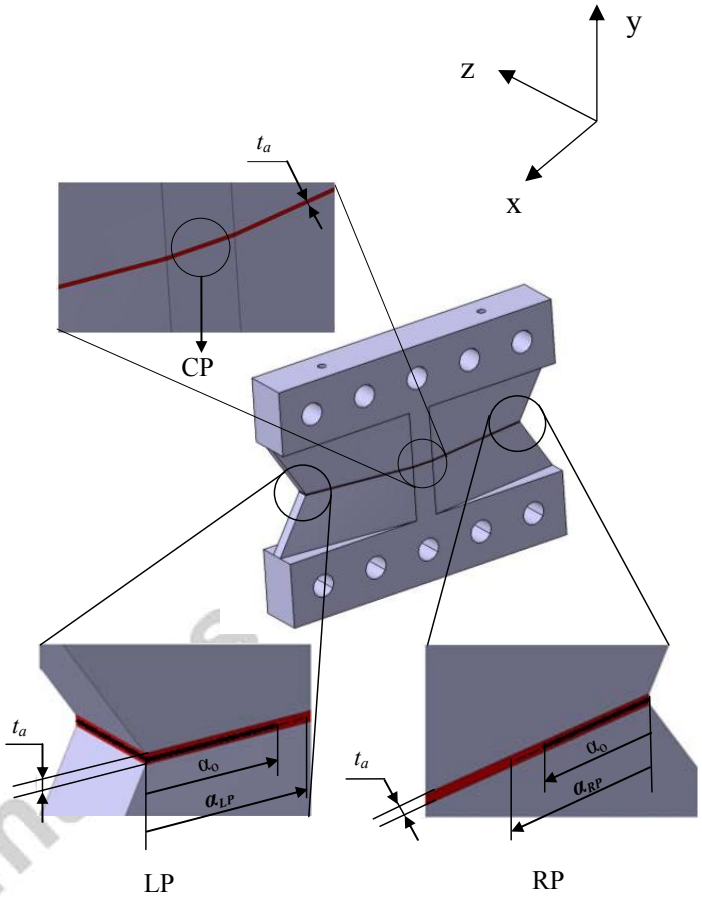

(b)

CP : Specimen Center Part

LP : Specimen Left Part

RP : Specimen Right Part

y: Out-of-plane tensile-compression axis of the adhesive layer

x: In-plane shear axis of the adhesive layer

z: In-plane transverse-shear axis of the adhesive layer

a_o = pre-crack length

a_{LP} = propagated crack length at LP

a_{RP} = propagated crack length at RP

t_a = adhesive layer thickness

(b) CP LP RP

Figure 2: a) Schematization of the substrate and main dimensions (in mm, tolerances at ± 0.05 mm), b) Schematization of the fully assembled specimen with pre-cracks.

The pairs of substrates were bonded separately to assure optimum control of the parallelism between their sections and of the adhesive layer thickness (t_a, figure 2b). An appropriate assembly was designed for this purpose, allowing for a uniform pressure to be applied along the joint during curing. The value of t_a was set at 0.5 mm by means of stainless steel precision thickness gauge strips. The surfaces to be joined were first ground with a 180 grit Silicon

Carbide (SiC) paper and then cleaned by 99% pure acetone. Any remaining residues were removed by oil-free compressed air. The SikaPower®-498 adhesive was applied by means of a wooden spatula. The pre-cracks were created using an aluminum foil of 0.011 mm thick, pre-coated on both sides with Silicone Paste 70 428 (used for lubrication in the food industry) in order to avoid any bonding with the adhesive bulk material. The foil was placed after application of the adhesive and before bringing the two substrates face to face. Its exact location has been marked on both sides of each substrate using gauge calipers. After full preparation of the bond, the specimens were conditioned in a 180 °C pre-heated furnace for 1 hour, following the instructions provided by the supplier. At the end of the curing process, they were left to cool at ambient temperature. Any adhesive excess was then removed using a 180 grit SiC paper and the finishing was done with a 1200 grit SiC paper. Before performing the tests, the thickness of the adhesive at CP, LP and RP was checked using a Nikon profile projector (model V-12B), and it was found to be in the range of 0.5 ± 0.05 mm.

3. Experimental procedure

The experiments were performed using a universal hydraulic tensile machine (figure 3). All specimens were loaded under displacement control at 0.5 mm/min until rupture. Four different phase angles (γ, see also figure 1) were tested: 0° (tension), 45° (tension/shear), 90° (shear) and 135° (compression/shear). The displacement field along the adhesive joint was measured using an image correlation system placed in front of each specimen (Aramis GOM 2M, figure 3a). On the rear side, a CCD camera (Qcam Retiga 1300 B, figure 3b) was used to monitor crack propagation at one extremity of the adhesive layer. To facilitate the detection of the crack tip during the tests, the back side of the joint has been painted white. All cameras were fully synchronized with the tensile machine so that with each recorded image, the

corresponding value of the applied force was also recorded. The specimens were mounted on the Arcan fixture by means of pins passing through the holes of each substrate (see also figure 2). Two pins were also used to connect the Arcan device with the hydraulic machine. The vertical alignment between these last two pins was also verified by means of a spirit level.

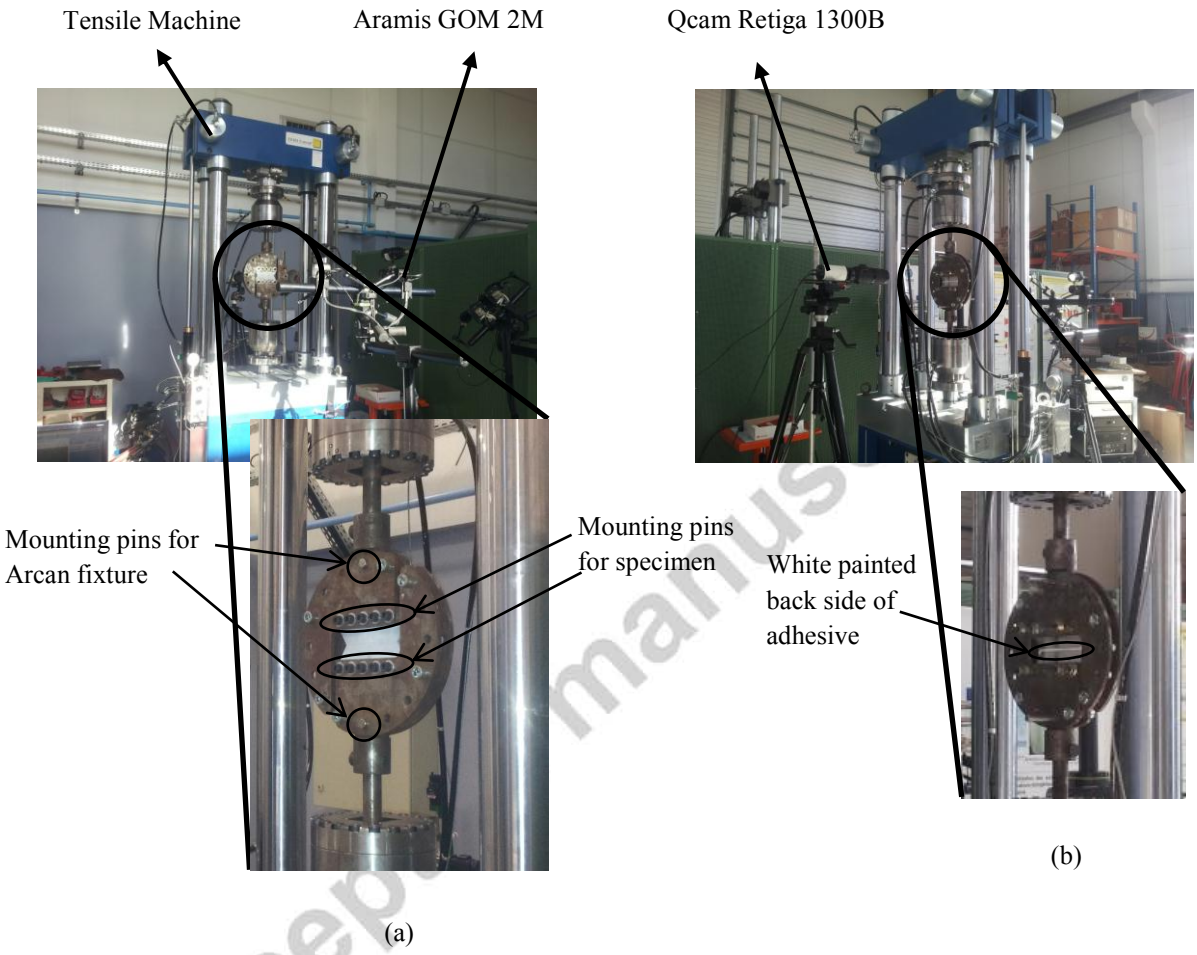

Figure 3: Experimental setup to perform the necessary experiments, with the Arcan fixture configured for a pure tensile test (0^o phase angle): a) Front view, b) Rear view.

4. Preliminary study

Before proceeding with the main study, it is necessary to define the appropriate value for the pre-crack length (a_o, see also figure 2b). Thus, a preliminary number of experiments have

been realized at the loading speed of 0.5 mm/min. The Aramis GOM 2M system was used to measure the relative displacement between the two substrates at CP, LP and RP (see also figure 2b). For reasons of simplicity, this "relative displacement" will be referred to as "displacement" here. Firstly, two specimens with no pre-cracks were tested, one at 0° and the other at 90°. The results at 0° showed that the displacements at rupture at RP and LP were higher than at CP. This phenomenon can be attributed to the difference in the width of the adhesive layer (5 mm at LP and RP contrary to 20 mm at CP, see also figure 2a). At 90°, the force-displacement curves at CP, LP and RP were identical. The forces at break for the tests at 0° and 90° were measured to be about 58 and 56 kN respectively.

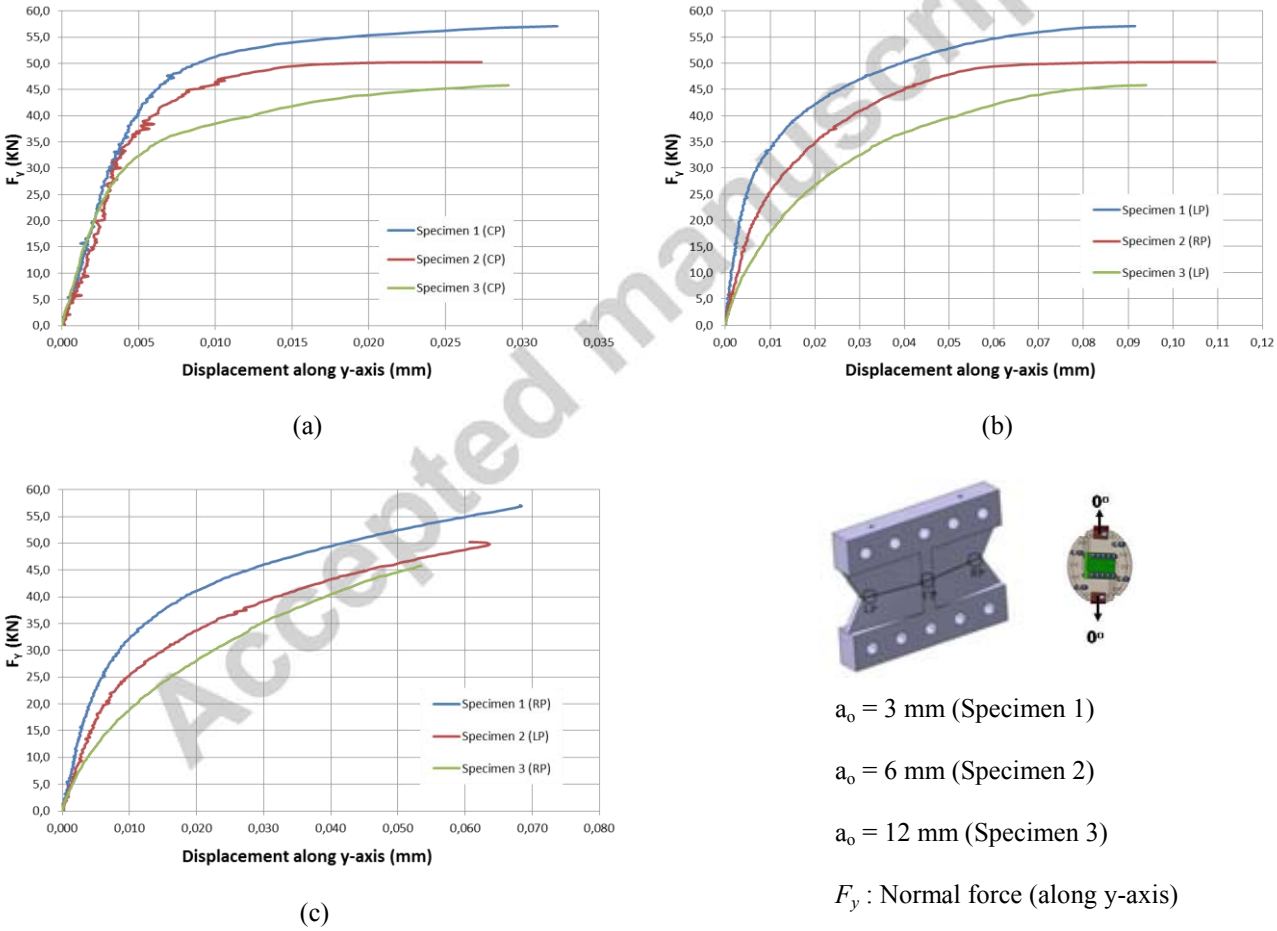

Figure 4: Force-displacement curves for specimens with different values of a_o at: a) CP, b) Most elongated extremity, c) Less elongated extremity.

After taking into account the previous observations for the un-cracked specimens, it was decided to determine the appropriate value of a_o by performing tests at 0°. Three lengths of a_o at 3, 6 & 12 mm were examined, and the results are given in figure 4. The graphs show, as was mentioned before for the un-cracked specimens, that LP and RP elongate more compared to CP. However, the force-displacement curves at LP and RP are not identical, in spite of the symmetric form of the specimens (see also figure 2b). Moreover, it is not always the same extremity that is more or less displaced: for specimen 2 the RP elongates more (around 0.11 mm), contrary to LP for specimens 1 and 3 (around 0.09 mm for both tests). The increased displacement of RP for specimen 2 causes also the displacement at LP to change direction (from tension to compression), after a certain force level close to the force at break (red curve, figure 4c). This is not apparent for the other two specimens. These phenomena could be attributed to variations in the homogeneity of the adhesive layer from the LP to the RP part, to small differences in the values of a_o, and/or to the appearance of some interface cracks before break. Thus, it is convenient to compare the more elongated extremities separately from the less elongated ones, as has been done for the results in figures 4b-c. Nevertheless, in order to avoid confusion, for the results of the main study, the more elongated part will be referred to as RP and the less elongated one as LP. Consequently, considering all these observations, when modeling the fracture of the joint at 0°, a particular attention needs to be taken in the definition of the boundary conditions.

At LP and RP (figures 4b-c), a clear influence of the value of a_o on the resulted force-displacement curves can be remarked: for the same level of the applied displacement the force decreases when increasing a_o. This is the case for the CP too (figure 4a), but for displacement values higher than around 0.003 mm. Until then, the force-displacement curves at CP are superposed. The test for a_o = 3 mm induces a very small difference in the break force (around

57 kN) compared to the un-cracked specimen (around 58 kN, as it was mentioned before). Therefore, it is not certain that such a small crack could produce a significant influence in the overall behavior of the adhesive joint, or that it could propagate in a stable manner during the experiment. On the other hand, when increasing the pre-crack to a_o = 12 mm, there is a large decrease in the break force (to around 46 kN). However, for this case, the curves at the LP and RP show practically no linear initial part. Thus, based on all these preliminary results, it has been decided to set $a_o = 6 \pm 0.5$ mm for the tests of the main study (the interval of ± 0.5 mm is added to account for variation in specimen preparation). Therefore, specimen 2 will be retained for the calculations of G_C along with the other tests performed in the main part of the study.

5. Results at phase angles 0° to 90°

5.1 General

The tests in the mixed mode I/II plane were performed as follows: 2 tests at 0° (Specimens 4-5), 2 tests at 45° (Specimens 6-7) and 1 test at 90° (Specimen 8). Figures 5 to 7 show the resulted force-displacement curves at CP, LP and RP. At 0° and 90°, F_y and the tangential force (F_x) are plotted as a function of the displacements along the y and x-axis respectively (see also figures 2 & 4). At 45°, both the normal and tangential to the adhesive layer force-displacement curves need to be presented. At this phase angle it is obvious that F_y and F_x are equal to the experimentally measured force divided by $\sqrt{2}$. In addition, it is shown on all graphs of figures 5 to 7 the force-displacement levels to which the fracture toughness for each experiment has been calculated. The choice of their position will be justified in the discussions to follow.

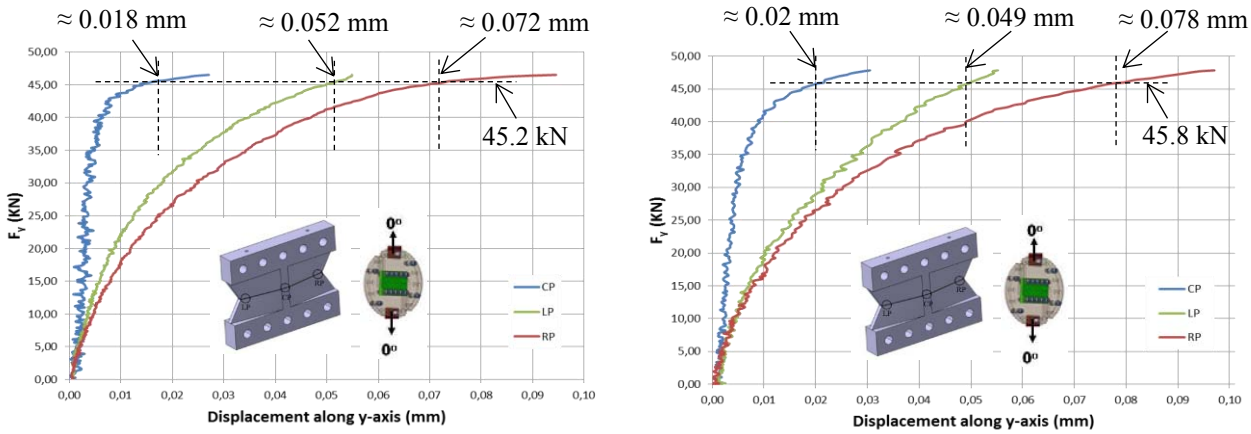

Figure 5: Force-displacement curves for tests at 0°: a) specimen 4, b) specimen 5.

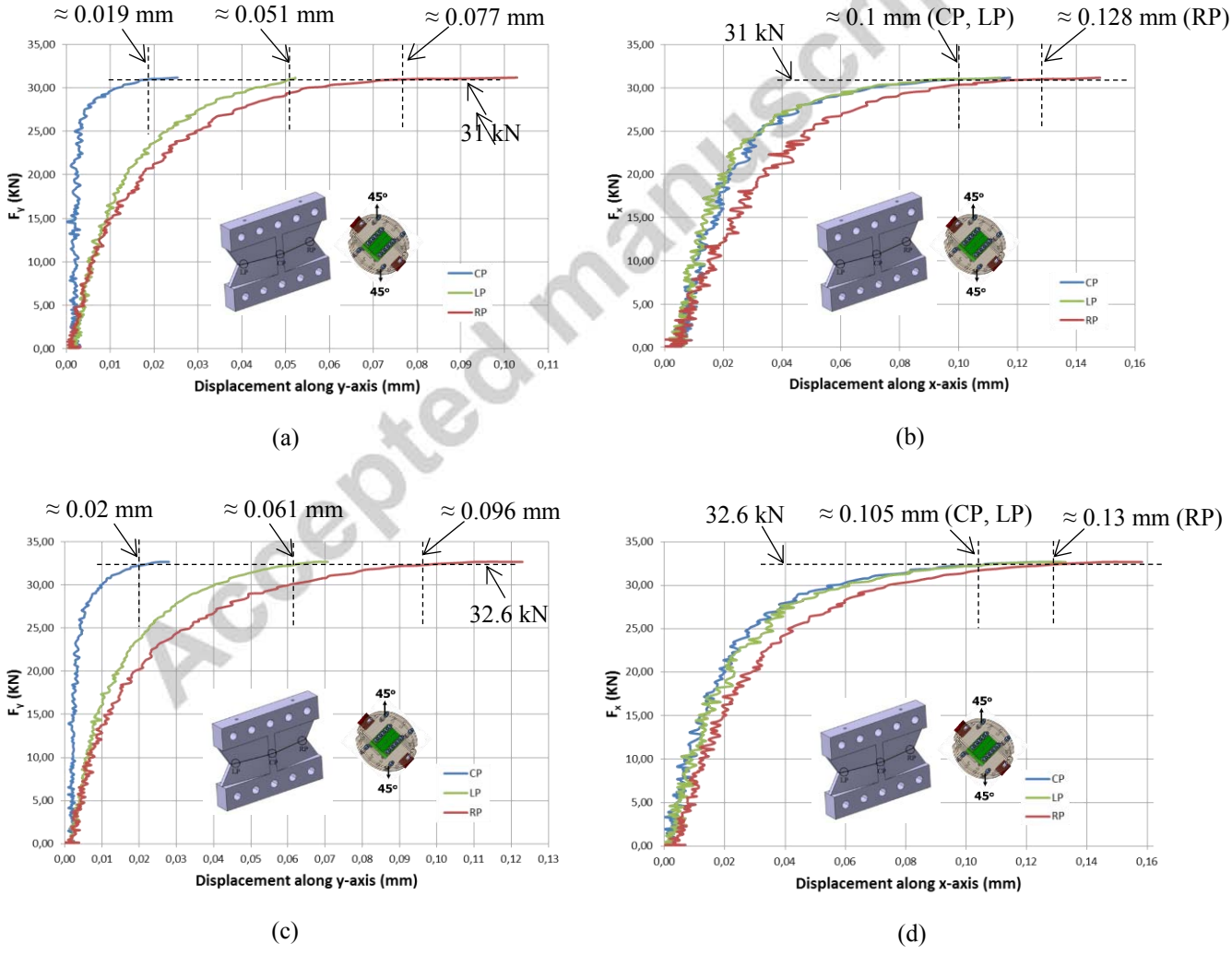

Figure 6: Force-displacement curves for tests at 45°: a) & b) specimen 6, c) & d) specimen 7.

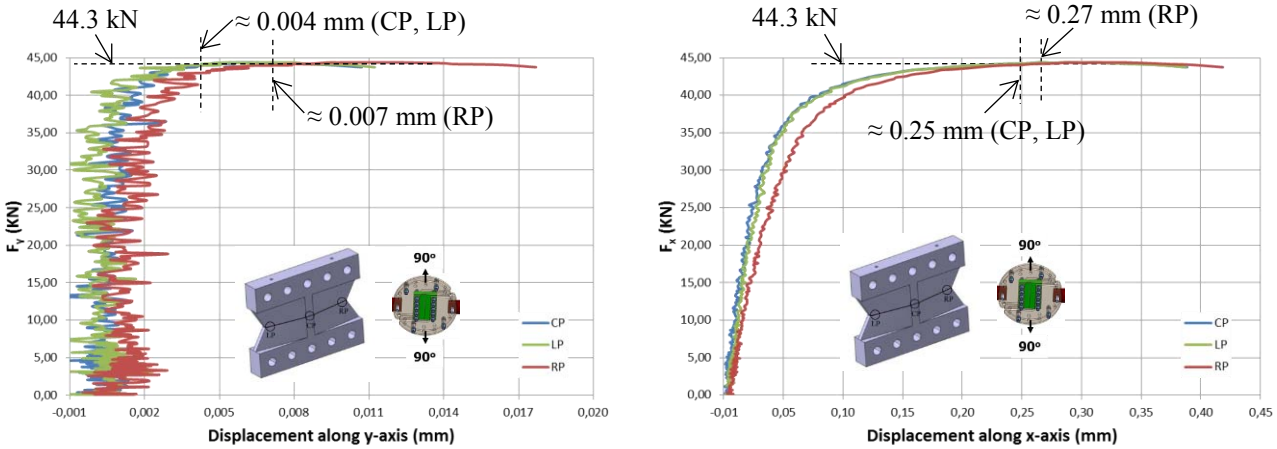

(a) (b)

Figure 7: Force-displacement curves for test at 90° (Specimen 8).

The normal force-displacement curves at 0° and 45° (figures 5a-c & 6a-c) show for both tests performed that, for the same force level, the displacement at CP was always lower comparing to the ones at LP and RP. In addition, the normal displacements at RP and LP were identical only at low force values (inferior to around 10 kN). These phenomena are in accordance with the previous discussions in the preliminary study section. However, contrary to what has been observed for the un-cracked specimens (see paragraph 4), the tangential force-displacement curves at CP, LP and RP are not identical (figures 6b-d & 7b). At 45°, it is interesting to note that, for both tests realized, the more elongated extremity in the tangential direction (referred as RP to facilitate the comparisons) was the same with the one in the normal direction. At 90°, a significant value of the normal displacement at rupture was measured (around 0.017 mm, figure 7a). This is not the case at 0°, where the tangential component of the displacement remained always at non-significant values until break (lower than 0.003 mm for both tests). The experimental values of the force at break at 0°, 45° and 90° were measured at around 47, 46 and 44.6 kN respectively.

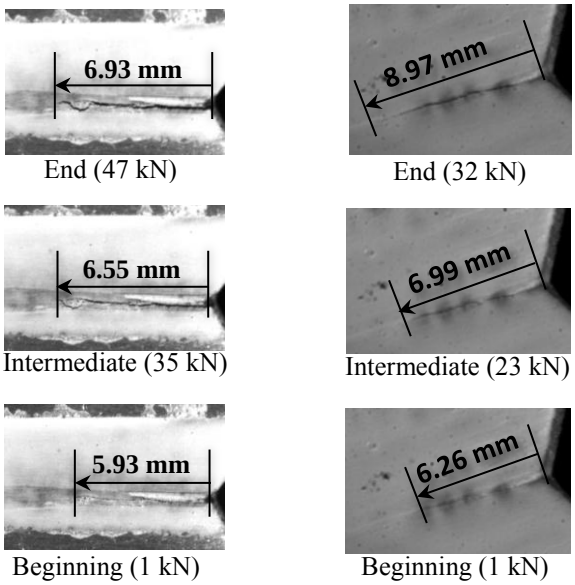

Figure 8: Crack propagation during the tests performed at a) 0° (specimen 4, 1 pixel = 0.023 mm^2) and b) 45° (specimen 6, 1 pixel = 0.029 mm^2).

Figure 8 shows the propagation of the crack for the tests performed at 0° (specimen 4) and 45° (specimen 6), as recorded by the Retiga 1300B camera (see also figure 3b). These results are very representative of the experiments performed on the specimens with $a_o = 6 \pm 0.5$ mm at the same phase angles. The behavior of the crack tip is presented at three different stages: the beginning of the experiment (taken at a force value of 1 kN), an intermediate point (the force level where the "first" apparent increase of the crack length was captured by the camera), and the break force. The results show that stable crack propagation took place before complete failure. In particular, for specimen 6 the crack length increased from 5.93 mm to 6.93 mm, and for specimen 8 from 6.26 mm to 8.97 mm. Moreover, it can be noted that the crack propagated inside the adhesive layer and not at the interface between the adhesive and one of the two substrates. Contrary to 0° and 45°, at 90°, no crack propagation has been seen on the surface of the specimen before complete failure. In addition to all these observations, it

must be mentioned that the rupture at the three previous phase angles was always cohesive. An example of the failure at 0° is given in figure 9 (specimen 4).

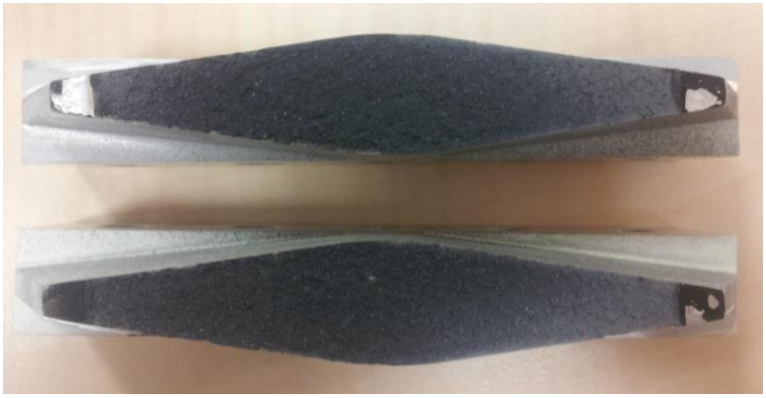

Figure 9: Example of failure at 0° (specimen 4).

5.2 Calculation of G_C using Finite Elements

The calculation of G_C was based on the LEFM theory here using the domain contour integral method (firstly introduced in an analytical form by Rice [30]). This was done despite the fact that the response of the SikaPower®-498 was clearly non-linear during the Arcan tests (see figures 4 to 7), in order to properly compare with the results of the TDCB-MMB tests [9] performed on the same adhesive. In particular, since SikaPower®-498 has been referenced as a "crash optimized" adhesive, it shows important non-linear behavior during the "classical" fracture mechanics tests too. This can be justified by the very high values measured for G_C (around 3 and 11 N/mm for the mode I & II load cases respectively, see [9]) in combination with the low yield strength of this adhesive (around 17 MPa measured at a loading rate of 0.5 mm/min, see [31]). Hence, the calculations of G_C using the formulae provided by the standards [2]-[6] include also the energy dissipated due to plasticity of the adhesive. The same assumption has been made for the Arcan tests too, since otherwise the comparison with the

TDCB-MMB tests would have simply been "non-applicable" for the case of the SikaPower®-498 adhesive.

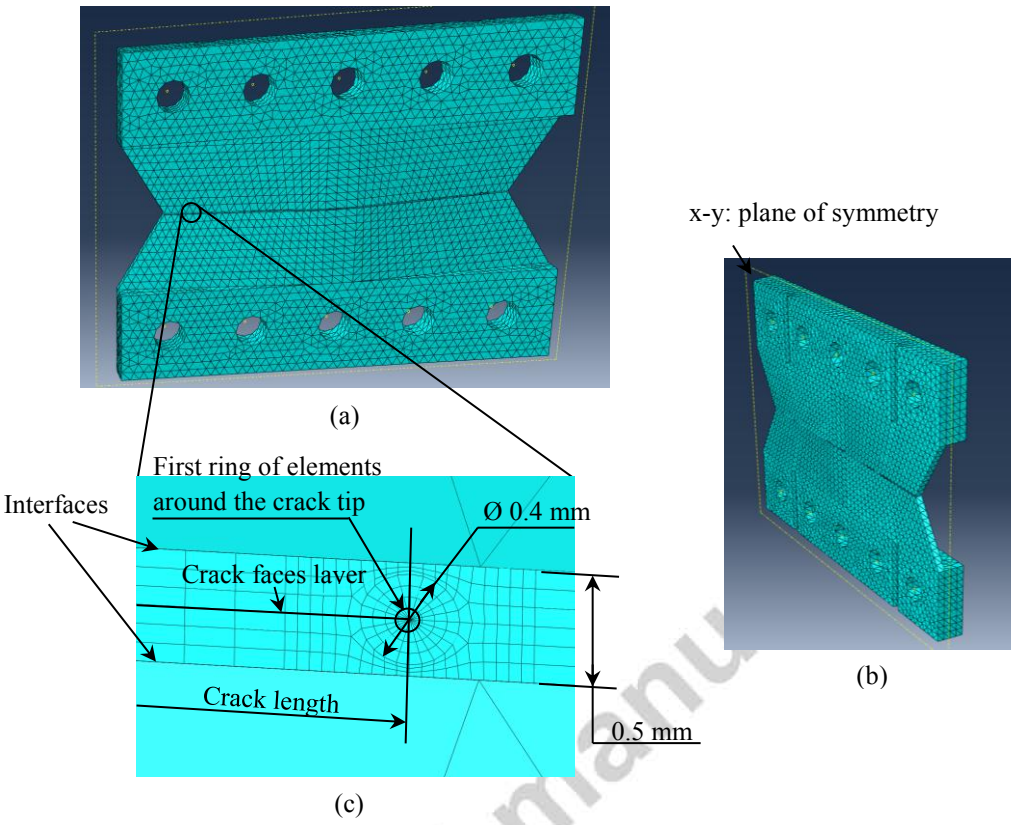

Figure 10: General overview of the finite element model, a) front view, b) side view showing also the symmetry plane and c) detail of the mesh around the crack tip.

The simulations were performed using the Abaqus™ Ver.6.12-1 software. Due to the particular form of the section of the substrates, it has been preferred to create a 3D model here (figure 10). However, in order to minimize as much as possible the simulation time, half of the specimen was created. Thus, the necessary antisymmetric boundary conditions along the z-axis were defined (x-y is the plane of symmetry, figure 10b). Both the substrates and the adhesive layer were modelled as linear, elastic and isotropic solids. The Young's modulus and the Poisson coefficient were set in accordance with the values from the previous study [9]: for

Aluminum 2017A (substrates) at 72.5 GPa and 0.33 respectively, and for SikaPower®-498 (adhesive) at 2.12 GPa and 0.36 respectively. Additional information about the mechanical properties of the substrate material can be found in [9] and of the adhesive under investigation in [31].

As shown in figure 10c, the substrates were modelled using linear tetrahedral elements (code Abaqus™ C3D4), and the adhesive layer with linear, fully integrated hexahedral ones (code Abaqus™ C3D8). Due to the inhomogeneous mesh between the adhesive and the substrates, tie conditions (which constrain the translational and rotational degrees of freedom of a pair of surfaces to be equal) were used at their interface. Along the z-direction of the adhesive layer, 50 elements were used for the half model presented in figure 10b. The crack was modelled assuming that it behaves in the same manner on both the front and back sides of the specimen during the test. Thus, the crack faces were created as having a trapezoidal form with the crack tip being a straight line along the z-axis. Their configuration under mode I was realized using the option "seam" crack of Abaqus™, which simply doubles the nodes of the faces of the elements that belong to the crack faces. At mode II, in order to avoid interpenetration, the crack faces were created manually and a frictionless contact between them was defined (this has been performed for the tests at 135° too). The crack front was represented by a circular cylindrical partition of 0.4 mm of diameter created inside the adhesive layer. The value of this diameter has been checked so as to include the zone of singularity around the crack tip and to ensure convergence of the domain contour integral method. The first ring around the crack tip was meshed using linear wedge Abaqus™ C3D6 elements.

The simulations were performed under displacement control. The necessary boundary conditions were applied on datum points defined on the x-y plane (figure 10b) and at the

center of the mounting holes (A to J, figure 10a). These points were connected to the appropriate parts of the cylindrical surfaces of the substrates (colored in pink, figure 11) by means of kinematic coupling constraints, according to the load case examined. On the substrate to be loaded, the appropriate datum points were linked with the upper half cylinder for the tensile load case and the right half cylinder for the shear load case. On the other substrate, the opposite cylindrical surfaces respectively were connected with the corresponding datum points to apply the reactions. At the reaction points, in order to simulate the fixing of the substrate via the mounting pins (see also figure 3a), the displacements along the x and y-axis and the corresponding rotations around them, were set equal to zero.

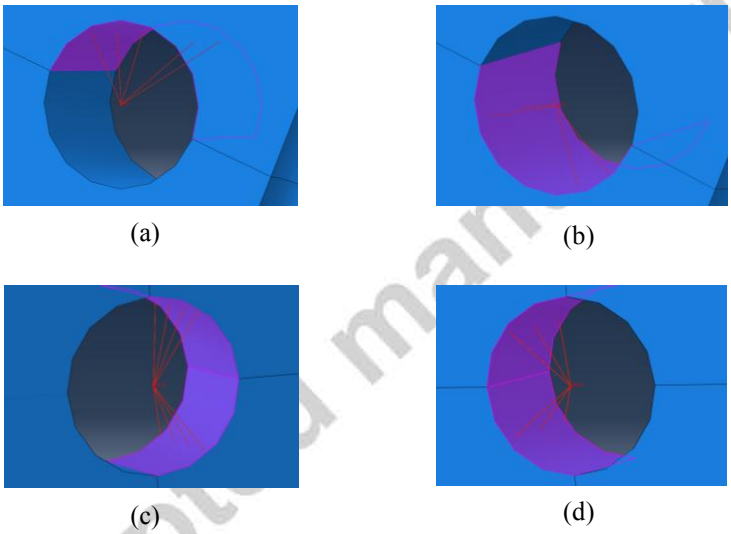

Figure 11: Kinematic coupling constraints to apply the boundary conditions: a) & b) load and reactions under tensile load, c) & d) load and reactions under shear load.

The Rice method [30] permits to calculate the energy dissipated at crack propagation (that is the energy release rate G), which for the linear elastic case considered here equals to G_C. Thus, in the discussions to follow, where necessary, G is used at the place of G_C for the illustration of the methodology developed. The methodology requires two main parameters to be properly adjusted: the crack length value and the mode mixity at the crack front. The direct

use of an experimental value of the crack length measured at the surface of the specimen (see also figure 8) in the numerical model, would imply the existence of a negligible non-linear area ahead of the crack tip. This is inappropriate since, due to the high fracture toughness values already identified for the SikaPower®-498 adhesive (see [9] and [28]), a large zone of micro-fibrillation must be expected at the crack front. Thus, the crack lengths to calculate G must be defined differently. As far as the mode mixity is concerned, it is convenient to consider pure mode I and II load cases at the crack tip when at 0° and 90° respectively. However, mode partitioning at 45° needs to be investigated. In addition, the edge effects, highly present when performing tests with the Arcan fixture [17], are expected to influence the computation of G and they must also be compensated.

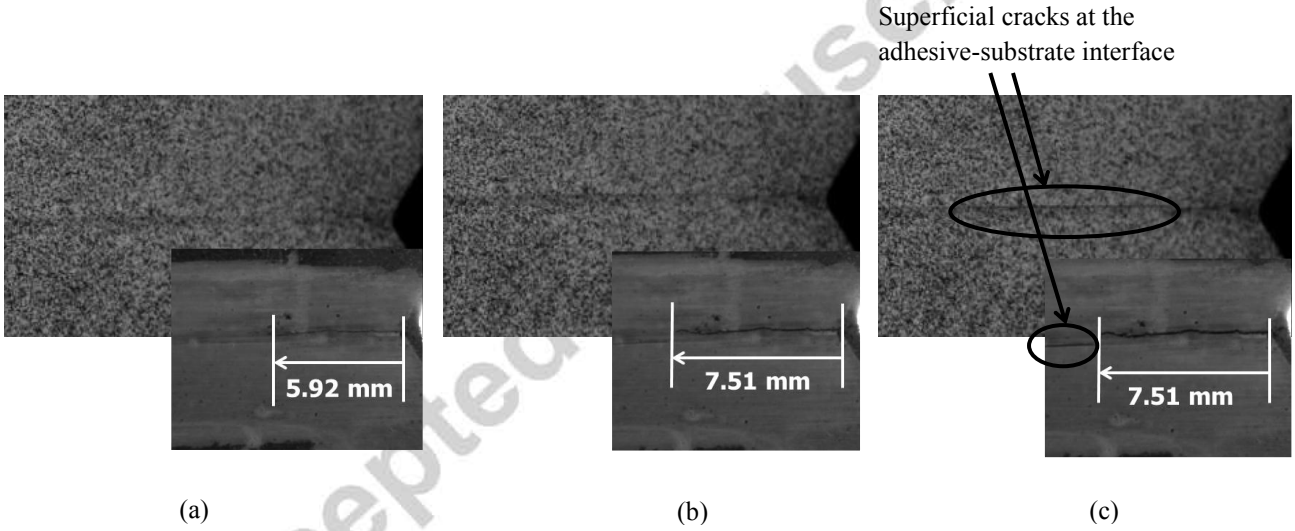

Figure 12: Example (specimen 2) of superficial interface cracks under mode I: a) beginning of the experiment, b) Force level retained to calculate G, c) break point.

In order for all the previous issues to be addressed, an alternative methodology has been developed. At first, it was defined the instant during the experiments to realize the calculation of G. At 0°, the examination of the images registered during the tests revealed the appearance of superficial cracks at a large length along the adhesive-substrate interface, after an

"elevated" force level and before break. This phenomenon must be related to the edge effects. An example is shown in figure 12 for specimen 2. Thus, for all tests at 0° the point just before the appearance of the superficial interface cracks was retained for the simulations. At 45° and 90°, no such cracks were detected by any of the optical systems used in this study. However, since it is difficult to exclude the influence of the edge effects on the Arcan tests, it was decided to perform the computation of G at the point just before the peak force for these two phase angles. At 90°, the normal force-displacement curve (figure 7a) was also used to ensure that the displacement along the y-axis at the previous point at CP, LP and RP, found between 0.004 and 0.007 mm, can be neglected. The exact points on the force-displacement curves that were retained for the simulations are given in the graphs of figures 5 to 7.

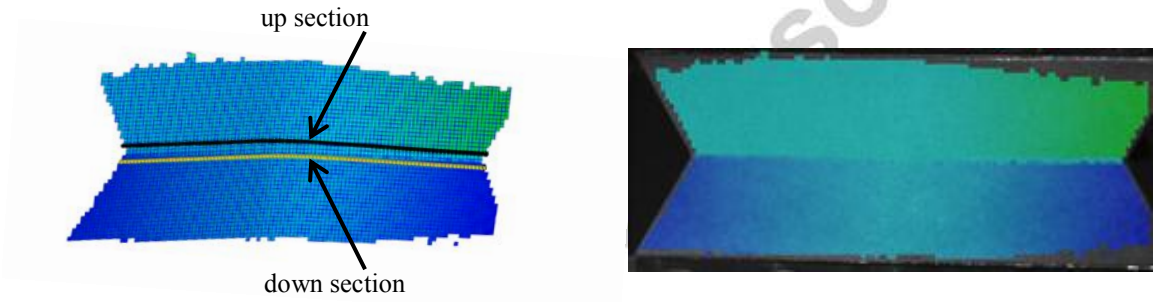

(a) (b)

Figure 13: Specimen 2, force level of 48.5 kN: a) location of the section where the displacement was measured (up section) and the reference (down section) was taken, b) superposition of the correlated area and the real image (1 pixel = 0.082 mm^2).

At the points on the force displacement curves previously identified, the next step consisted of calibrating the lengths of the cracks a_{LP} and a_{RP} (see also figure 2b). In order to achieve this, by using the data from the image correlation system (see also figure 3a), it was measured the relative displacement between the sections of the two substrates at the instant retained. At 0° and 90° the displacements along the y and x-axis respectively were used for this computation,

and at 45° the ones along both of them. This operation also allowed for the necessary mode partitioning at 45°. The sections of the substrates were defined as close as possible to the adhesive-substrate interface (figure 13). Since the measurements were performed on the surfaces of the specimens, it is necessary to presume for all the tests that the previously calculated displacement is similar along the width of the adhesive layer (the z-axis, see also figure 10). In figures 14 to 16 it is plotted for all the tests the evolution of this displacement as a function of the x-coordinate of the points constituting the up section (blue curves, the origin of the x-axis is presented in figure 10). When under mode I (figures 14, 15a and 15c), the experimental curves have a parabolic form, with the minimum displacement being at the CP of the joint and the maximum one at the RP. When under mode II (figures 15b, 15d and 16), the displacement along the joint is almost constant, with slightly elevated values, however, at RP. These results for all three phase angles are in agreement with the previous discussions in this paper.

The above experimental curves were approximated by finite elements in order to calculate G. Several simulations for each test have been realized by varying: the displacement at the loading holes (A to E, figure 10a), and the lengths of the cracks a_{LP} and a_{RP}. When under mode I at 0° and 45°, the simulations were repeated until the relative displacement along the y-axis at the adhesive-substrate interface in the numerical model agreed with the corresponding experimental data at CP, LP and RP. At the same time, the sum of the forces on the reaction points (holes F to J, figure 10a), was checked to be equal to the force level retained experimentally for the simulations as described above. However, when under mode II at 45° and 90°, the best approximation of the experimental curves has been obtained only when considering no crack propagation. For this load case, simply the displacement values along the x-axis on the loading holes were adjusted, until the relative displacement of the

adhesive-substrate interface in the numerical model agreed with the corresponding experimental data at CP. At 45°, the identified values of a_{LP} and a_{RP} for the mode I portion of the load were also used for the simulations under shear loading. At 90° both values of a_{LP} and a_{RP} were left equal to 6 mm. The results obtained after applying the methodology described above are shown in figures 14 to 16 (brown curves). The details concerning the calibrated crack lengths a_{LP}, a_{RP} and the calculated values for G, are given in table 1. It can be noticed that the calibrated crack lengths for the mode I load case are much higher than the experimentally measured ones (see also figure 8). In addition, it should be mentioned that the energy release rate has been calculated on the plane of symmetry x-y (that is at z = 0 mm, see also figure 10b) and in the middle of the thickness of the adhesive layer.

Specimen number	Phase angle	Force level retained to perform the simulations		a_o (mm)	Calibrated crack lengths		Calculated fracture energy G			
		F_x (kN)	F_y (kN)		a_{LP} (mm)	a_{RP} (mm)	G_{IL} (N/mm)	G_{IR} (N/mm)	G_{IIL} (N/mm)	G_{IIR} (N/mm)
2	0°	-	48.5	6	14	14	2.98	2.98	-	-
4	0°	-	45.2	6	12	18	2.31	3.35	-	-
5	0°	-	45.8	6	15	23	2.38	3.45	-	-
6	45°	31	31	6	10	16	1.98	2.97	1.70	3.12
7	45°	32.6	32.6	6	10	24	2.81	3.06	1.77	3.17
8	90°	44.3	44.3	6	6	6	-	-	12.03	13.12

G_{IL}, G_{IR}: Fracture energies calculated for the left and right cracks respectively when under mode I load case

G_{IIL}, G_{IIR}: Fracture energies calculated for the left and right cracks respectively when under mode II load case

Table 1: Energy release rate calculated for the SikaPower-498® at 0°, 45° and 90° (G = G_C).

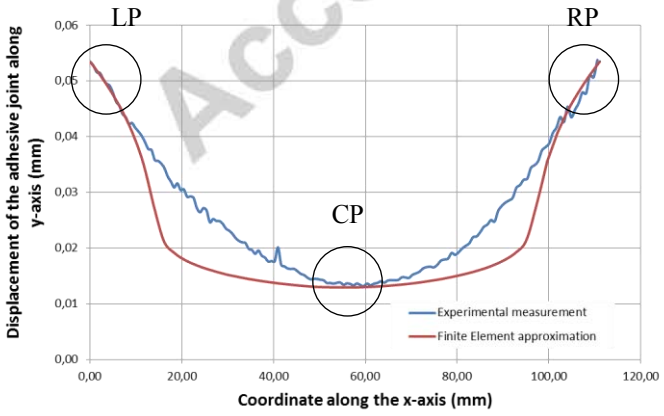

(a)

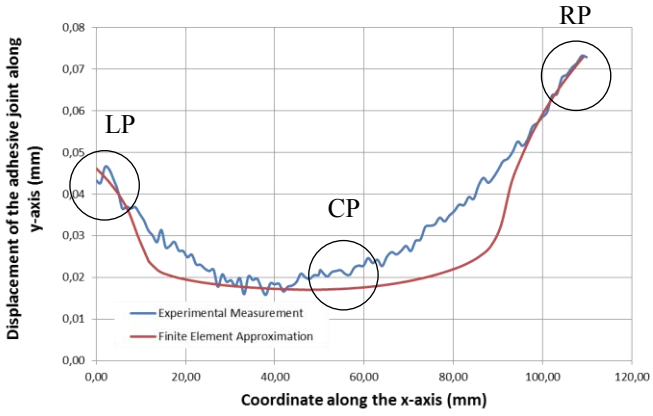

(b)

(c)

Figure 14: Approximation of the displacement applied along the y-axis on the adhesive layer at 0° by finite elements: a) specimen 2, b) specimen 4 and c) specimen 5.

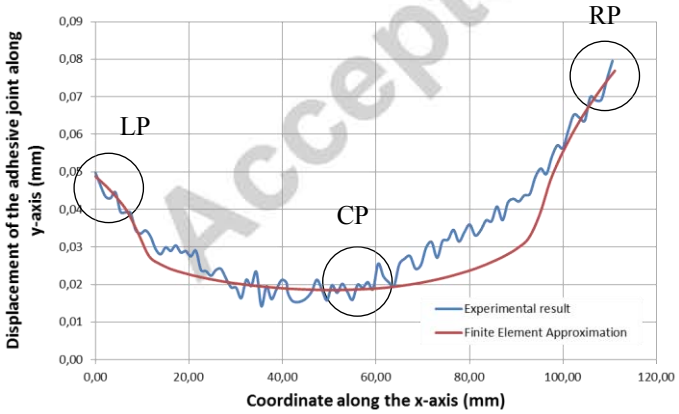

(a)

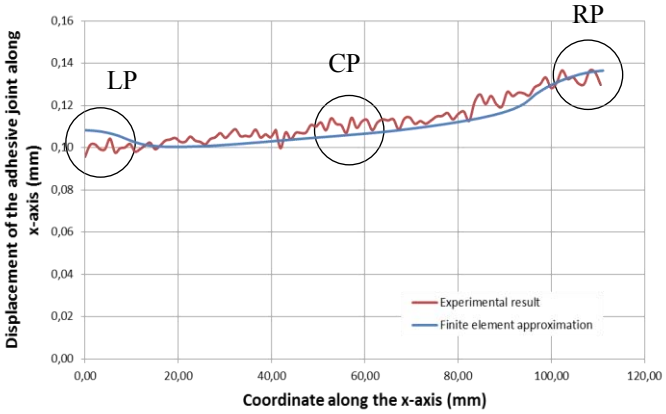

(b)

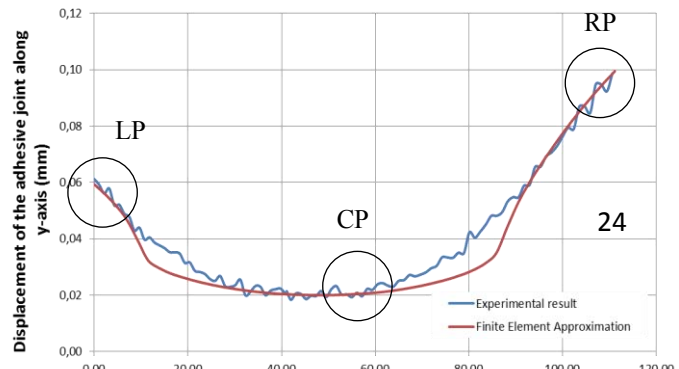

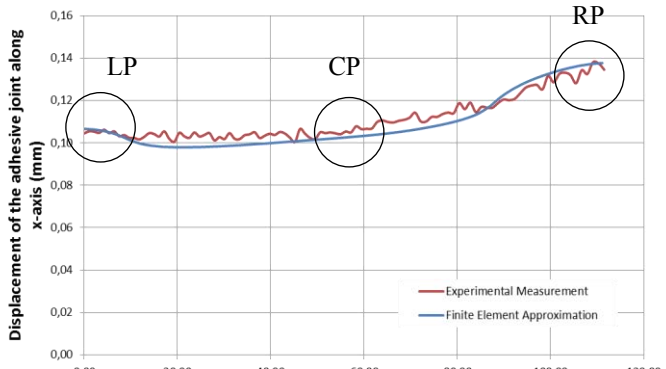

(c) (d)

Figure 15: Approximation of the displacement applied on the adhesive layer along the y and x-axis at 45° by finite elements: a) & b) specimen 6, c) & d) specimen 7.

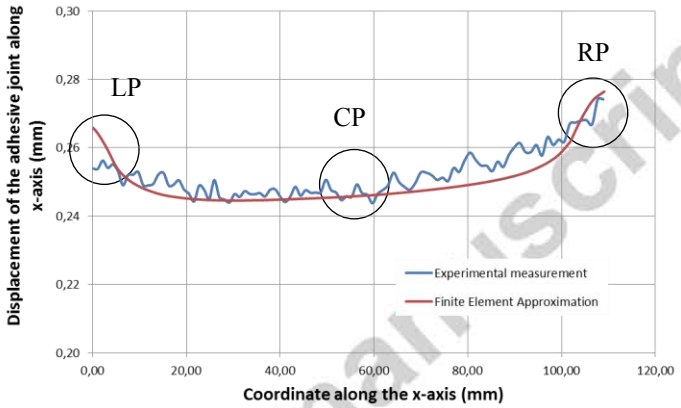

Figure 16: Approximation of the displacement applied on the adhesive layer along the x-axis at 90° by finite elements (specimen 8).

The methodology described above for calibrating the crack lengths a_{LP} and a_{RP} at mode I (figures 14 & 15a-c), resulted to a very good approximation of the experimental curves at CP, LP and RP (the position of CP, LP and RP is also given in all figures 14 to 16). There exists, however, a difference in the intermediate parts (transition area from LP to CP and from CP to RP). This could be explained in different ways. Firstly, it must be noted that the behavior of the adhesive during the tests was strongly non-linear. In addition, non-linear behavior of the substrates could also have occurred. These two phenomena have not been taken into account in the numerical model. Moreover, even if the simulations to calculate G were performed before the peak force in order to eliminate the influence of the superficial interface cracks,

their existence at a smaller non-detectable degree prior to the force level chosen should not be excluded. A very good approximation has also been achieved for mode II loading at CP and RP (figures 16b-d & 17). The differences observed at LP could be attributed to similar reasons as for mode I. However, in the numerical model for the mode II load case, as it was mentioned earlier, a frictionless contact between the crack faces has been defined. Despite that, a small penetration of one crack face into the other could not be avoided. Thus, further research is needed on these last points. Nevertheless, this is out of the scope of the present paper. Finally, it must be noted that the use of finer mesh densities than the ones shown in figure 10 for the adhesive and the substrates, or the changing from linear to quadratic elements, had no significant effect on any of the above results (or on the ones given in table 1 for G).

The mean value of G_C for the mode I load case can be calculated at 3.26 N/mm using the results data in table 1. From this computation it has been excluded G_{IL} for specimens 4 and 5, since they have been found to be very low comparing to G_{IR} for both of them. Physically, this means that very little or no crack propagation occurred at the less elongated extremity of these specimens during testing, and that failure must have occurred with the crack propagating at the opposite extremity. For the two tests that have been performed at 45° a similar phenomenon was noted. The mean values for the mode I and II components of G_C at this phase angle have been found to be at 3.02 N/mm and 3.15 N/mm respectively, using only the data corresponding to the right crack. At 90°, there was no significant difference between the two values of G_{IIL} and G_{IIR}. Therefore, it can be considered that the value of G_C under mode II load was measured between 12.03 N/mm and 13.12 N/mm.

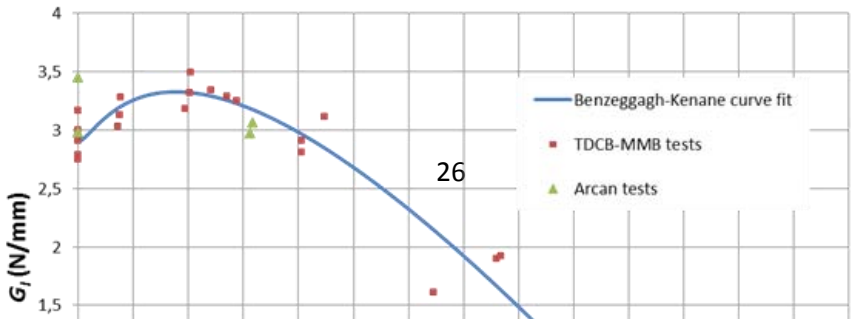

Figure 17: Comparison between the results from the TDCB-MMB [9] and the Arcan tests for the SikaPower®-498 adhesive (G_I, G_{II}: the mode I and II components of G_C respectively).

Figure 17 shows the comparison between the evolution of G_C in the mode I / mode II plane obtained for the SikaPower®-498 adhesive using the Arcan fixture, and the one from our previous study [9] by means of the TDCB-MMB tests. The Benzeggagh-Kenane [29] fitted curve as identified in [9] for the adhesive under investigation is also added in the graph. The low values for G_I and G_{II} calculated at 0° and 45° are excluded from the illustration in figure 17, for the reasons mentioned earlier. As a general observation, it can be noted that the values of G_C measured by these two types of testing were found to be very close to each other. The small differences that exist must be attributed to the nature of the two methodologies. For example, under pure mode I loading, the mean value of G_I calculated using the Arcan fixture is at 3.27 N/mm, which is slightly higher than the corresponding one found using the TDCB-MMB tests (at 2.93 N/mm, see [9]). According to the previous discussions, this increase could be attributed to the edge effects which disturb the Arcan tests. In addition, under pure mode II load, G_{II} was measured higher too than 11 N/mm (the value identified in [9]). This difference could also be caused by the mode I component of the displacement measured at the point retained for the simulations (see also figure 7). Moreover, as mentioned earlier in the

introduction part, the substrates used for the TDCB-MMB tests are vulnerable to non-linear behavior. This, however, is much less likely to occur during the Arcan tests, because of the larger width and/or height of the adherents (see also figure 2a).

At this point, it is important to make a comparison between the values of G_C calculated with the methodology proposed in this paper, and those that would have been obtained from a "simplified" analysis of the Arcan tests. Simplifying the computation of G_C would imply performing the simulation directly at the break point and considering no crack propagation (that is $a_{LP} = a_{RP} = 6$ mm). Applying this approach for specimens 2 (0°) and 8 (90°) for example, resulted in $G_I = 4.82$ N/mm and $G_{II} = 14.58$ N/mm respectively. These values for the two previous specimens are higher (see also table 1) from those calculated after using the methodology proposed in the present manuscript. A similar behavior must be expected for all the other the specimens. Thus, after also comparing with the results obtained using the TDCB-MMB tests, it can be concluded that it is extremely important to take the precautions proposed in the current study in order to analyze the results of the Arcan tests and measure correctly the G_C of an adhesive joint. Otherwise, it is most likely that erroneous results will be obtained.

6. Results at phase angle 135°

Using the modified Arcan fixture [12], it was also tested the effect of compression-shear load on the fracture toughness of the SikaPower®-498 adhesive. Two specimens were fabricated for the needs of this part of the study, having the same form as the one shown in figure 2, but at a smaller dimensional scale: the length of the section of the substrates has been reduced from 110 mm to 70 mm and their width increased from 20 mm to 25 mm. The rest of the

dimensions remained unchanged. The reason for modifying these dimensions was the fact that under compression shear loading the force at break increases to very high values. Therefore, if the same substrate geometry as the one designed for phase angles 0° to 90° had been used, it would have been necessary to stop the experiments before total failure of the joint, in order to prevent any damage on the Arcan fixture or even the tensile machine.

The force-displacements curves at CP, LP and RP are given in figure 18. The force values represented on the ordinates axis are the experimental ones divided by $\sqrt{2}$, as it was also done for the tests at 45°. It should be noted here that the normal components of the load and of the displacement are negative when at 135°. However, in order to facilitate the illustration, their absolute values are plotted in figures 18b-d. This is obviously not the case in the tangential direction (figures 18a-c). Since the normal load has a compressional direction it is not expected to have any effect in the value of G. In addition, the normal component of the displacement has a low value at rupture (less than 0.006 mm) compared to the tangential one (between 0.14 mm and 0.16 mm). Therefore, for the tests at 135°, the computation of G was performed only for shear loading. The graphs in figure 18 show also, for both tests at 135°, that it is the CP of the joint which is displaced the most comparing to the LP and RP, and this along both the x and y-axis.

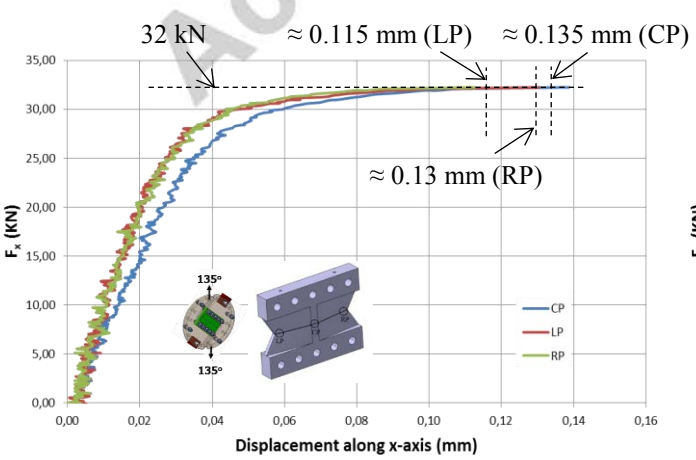

(a)

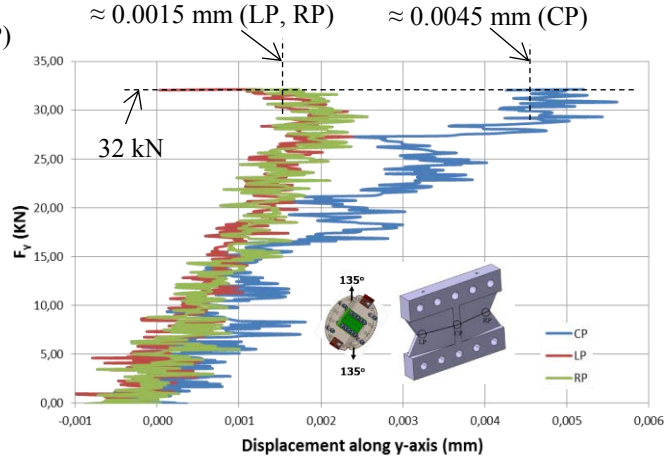

(b)

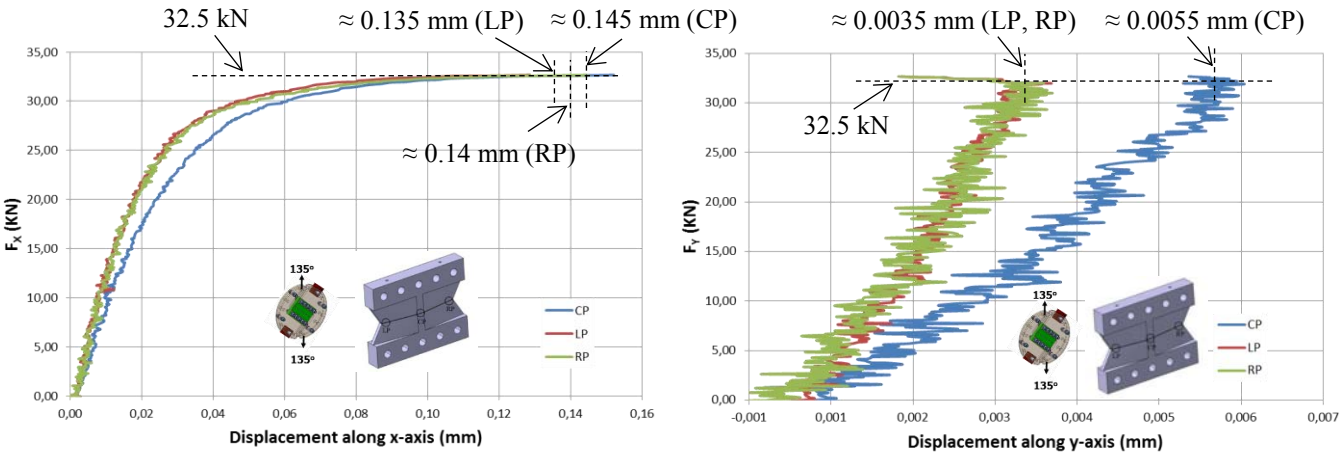

(c) (d)

Figure 18: Force-displacement curves for tests at 135°: a) and b) specimen 9, c) and d) specimen 10.

The same methodology as described above for the mode II load case was used to calculate G. The simulations were performed using the pre-crack length (at 6 mm, see also figure 2), since no crack propagation has been detected for the tests at 135°. The computation of G has been performed before the peak force (the force at break) and before the "abrupt" decrease of the normal component of the displacement (figures 18b-d). The exact points retained for the simulations are given on the graphs of figure 18. The approximation of the displacement field applied on the adhesive layer was performed for the CP part of the joint, and the result is presented in figure 19. The differences observed between numerical and experimental data at one of the two extremities (the RP) and at the transition parts (LP to CP and CP to RP), could be attributed to the same reasons as described above for the 0° to 90° load cases.

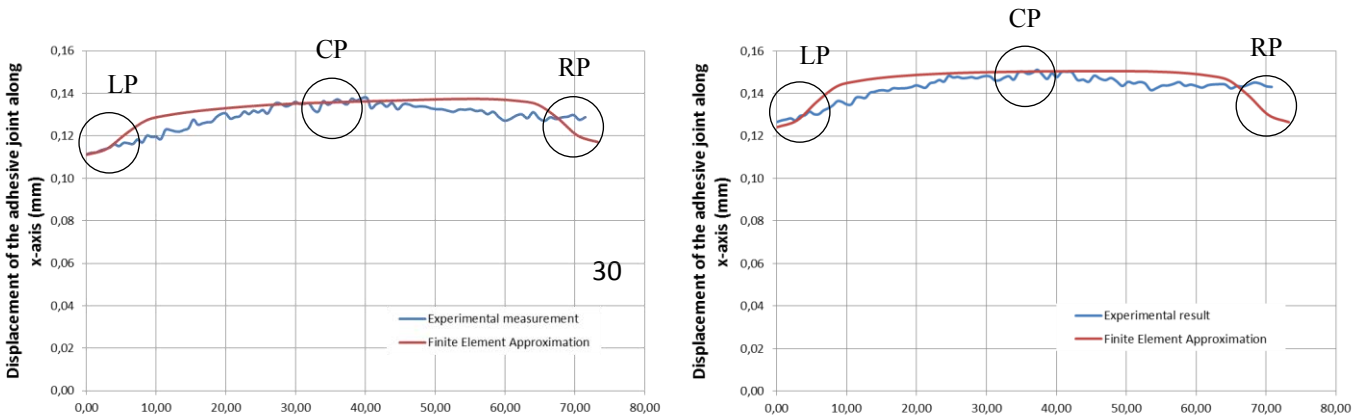

Figure 19: Approximation of the displacement applied on the adhesive layer along the x-axis at 135° by finite elements: a) & b) specimens 9 and 10 respectively.

Specimen number	Calculated facture energy G	
	G_{IIL} (N/mm)	G_{IIR} (N/mm)
9	16.53	15.30
10	19.97	18.39

Table 2: Energy release rate calculated for the SikaPower-498® adhesive at 135° ($G = G_C$).

Table 2 shows the results of the simulations for G at 135°. For specimen 9 the maximum value for G was calculated at 16.53 N/mm and the corresponding one for specimen 10 at 19.97 N/mm. These 2 values are much higher than the maximum value for G calculated for the test at 90° (13.12 N/mm). This means that the energy necessary to propagate a crack under compression/shear loading is much higher than the one needed under pure mode II. However, it must be mentioned here that the frictionless contact between the crack faces defined in the numerical model of the test at 135°, could explain this increase. Indeed, due to the compressional direction of the normal load, the energy dissipated by the friction between the two crack faces must be important. This energy is included in the results for G presented in table 2. It has not been subtracted since this has not been done for the tests at 45° and 90°, and

because this would require a thorough analysis of the nature of the contact between the two crack faces. The latter, despite its importance, is out of the scope of the present paper.

7. Conclusions and Perspectives

In the present study, the variation of the fracture toughness of the SikaPower®-498 adhesive was measured using the Arcan fixture. Four different phase angles have been examined: 0°, 45°, 90° and 135°. The specimens tested were fabricated using aluminum substrates with a specially designed section to allow for crack propagation. A methodology has been developed to calculate the fracture toughness, combining digital image correlation measurements and finite element modelling of the experiments. This technique was used to calibrate the crack lengths and perform the necessary mode partitioning at 45° and 135°. The comparison of the results on the mode I/II plane with the corresponding ones measured by the TDCB-MMB tests [9] performed on the same adhesive, showed good agreement. The variation observed has been mainly attributed to the difference in the nature of the two experimental techniques. At 135°, the fracture toughness has been found to increase beyond the values identified for the 90° phase angle.

It is important here to perform an evaluation of the methodology described in the manuscript, since its application is quite costly (Arcan fixture, special section of the substrates, digital image correlation system, camera to monitor the crack tip and finite element modelling). However, it is interesting to use since it bypasses the need for experimental measurement of the value of the crack length and allows mode partitioning to be performed. In addition, substrates made of high limit of elasticity materials are not required, as is the case mainly for the MMB test [9]. Moreover, the modified Arcan setup permits measurement of the fracture

toughness of the adhesive under compression-shear loading too, which is not possible to do with the standardized fracture mechanics tests. However, the Arcan tests are strongly influenced by the edge effects [17], and this has a direct influence on the calculated values of the fracture toughness. Even though care has been taken to overcome this issue by performing the computations before the force at break, undoubtedly, this solution needs to be improved.

The results presented in this manuscript are only the first ones using an alternative methodology. Thus, more experiments are certainly needed and also tests on other types of adhesives, if it is to be recommended to replace the standardized fracture mechanics tests to study the failure of adhesive joints. In addition, the influence of certain parameters on the values of the fracture toughness, which were excluded from the computations that have been performed here, must be examined. One of these is the non-linear behavior of the SikaPower®-498 adhesive, which has been identified by means of the Arcan fixture using a spectral viscoelastic law [31]. Moreover, it could be investigated the effect on the results of possible non-linearity of the material of the substrates, and, for the mode II loading, the friction between the crack faces. Finally, the influence of the loading speed on the fracture toughness is worth of examining too, since the SikaPower®-498 is considered to be a crash optimized adhesive. Some of these aspects are currently under investigation.

8. References

[1] Stigh U, Damage and crack growth analysis of the double cantilever beam specimen. Int J Fracture 1988;37:R13–R18.

[2] ASTM D3433-99. Annual book of ASTM standards, adhesives section 15. Philadelphia, PA: ASTM; 2012.

[3] ISO 25217:2009; 2009.

[4] BS 7991:2001; 2001.

[5] ASTM D6671/D6671M-13e1. Annual book of ASTM standards, Composite Materials section 15. Philadelphia, PA: ASTM; 2013.

[6] ISO/DIS 15114:2014; 2014.

[7] ASTM WK 22949. Annual book of ASTM standards, Composite Materials section 15. Philadelphia, PA: ASTM; (standard under preparation).

[8] Ducept F, Davies P, Gamby D, Mixed mode failure criteria for a glass/epoxy composite and an adhesively bonded composite/composite joint, Int J Adhes Adhes 2000;20:233-44.

[9] Stamoulis G, Carrere N, Cognard JY, Davies P, Badulescu C, On the experimental mixed-mode failure of adhesively bonded metallic joints, Int J Adhes Adhes 2014;51:148-58.

[10] Bascom WD, Timmons CO, Jones RL, Apparent interfacial failure in mixed-mode adhesive fracture, J Mater Sci 1975;10:1037-48.

[11] Davies P, Sims GD, Blackman BRK, Brunner AJ, Kageyama K, Hojo M, Tanaka K, Murri G, Rousseau C, Gieseke B, Martin RH, Comparison of test configurations for the determination of G_{IIC}: results from an international round robin, Plast Rubber Compos 1999;28(9):432-37.

[12] Blackman BRK, Fracture Tests. In: Lucas F.M. da Silva, Andreas Öchsner, Robert D. Adams, editors. Handbook of Adhesion Technology (Volume 1), Springer Heidelberg; 2011, p. 473-501.

[13] Adams RD, The Notched Torsion Test to determine the Mode III Fracture Properties of Adhesives. In: Lucas F.M. da Silva, David A. Dillard, Bamber R. K.Blackman, Robert D. Adams, editors. Testing Adhesive Joints, Wiley-VCH Verlag GmbH & Co.; 2012, p. 191-194.

[14] Andersson T, Stigh U, The stress–elongation relation for an adhesive layer loaded in peel using equilibrium of energetic forces, Int J Solids Struct 2004;41:413-34.

[15] Tamuzs V, Tarasovs S, Vilks U, Delamination properties of translaminar-reinforced composites, Compos Sci Technol 2003;63:1423-31.

[16] Arcan L, Arcan M, Daniel I, SEM fractography of pure and mixed mode interlaminar fracture in graphite/epoxy composites, ASTM Tech. Publ. 1987; 948: 41-67.

[17] Cognard JY, Davies P, Sohier L, Créac'hcadec R, A study of the non-linear behaviour of adhesively-bonded composite assemblies, Compos Part A-Appl S 2006;76:34-46.

[18] Taher ST, Thomsen OT, Dulieu-Barton JM, Zhang S, Determination of mechanical properties of PVC foam using a modified Arcan fixture, Compos Part A-Appl S 2012;43:1698-08.

[19] Sutton MA, Boone ML, Ma F, Helm JD, A Combined Modeling-Experimental Study of the Crack Opening Displacement Fracture Criterion for Characterization of Stable Crack Growth under Mixed Mode I/II Loading in Thin Sheet Materials, Eng Fract Mech 2000;66:171-85.

[20] Sutton MA, Deng X, Ma F, James C, Newman Jr., James M, Development and Application of a Crack Tip Opening Displacement-Based Mixed Mode Fracture Criterion, Int J Solids Struct 2000;37:3591-18.

[21] Jurf RA and Pipes RB, "Interlaminar fracture of composite materials," Journal of Composite Materials 1982;16(5):386-94.

[22] Pang HLJ, Mixed Mode Fracture Analysis and Toughness of Adhesive Joints, Eng Fract Mech 1995;51(4):575-83.

[23] Pang HLJ, Seetoh CW, A Compact Mixed Mode (CMM) Fracture Specimen for Adhesive Bonded Joints 1997;57(1):57-65.

[24] Choupani N, Interfacial Mixed-Mode Fracture Characterization of Adhesively Bonded Joints, Int J Adhes Adhes 2008;28:267-82.

[25] Choupani N, Mixed-Mode Cohesive Fracture of Adhesive Joints: Experimental and Numerical Studies, Eng Fract Mech 2008;75:4363-82.

[26] Choupani N, Experimental and Numerical Investigation of the Mixed-Mode Delamination in Arcan Laminated Specimens, Mater Sci Eng A 2008;478:229-42.

[27] Deepankar D and Narasimhan R, Analysis of an Interface Fracture Specimen for Adhesively Bonded Joints, Int J Fracture 1998;98:L35-L40.

[28] Marzi S, Anders B, Stigh U, On Experimental Methods to Investigate the Effect of Layer Thickness on the Fracture Behavior of Adhesively Bonded Joints, Int J Adhes Adhes 2011;31:840-50.

[29] Benzeggagh ML, Kenane M, Measurement of Mixed Mode Delamination Fracture Toughness of Unidirectional Glass/Epoxy Composites with Mixed-Mode Bending Apparatus, Compos Sci Technol 1996;56:439-49.

[30] Rice JR, A path independent integral and the approximate analysis of strain concentration by notches and cracks, J Appl Mech 1968;35:379-86.

[31] Badulescu C, Germain C, Cognard JY & Carrere N, Characterization and modelling of the viscous behaviour of adhesives using the modified Arcan device, J Adhes Sci Technol 2015;29(5):443-61.